Soft Matter

PAPER

View Article Online
View Journal | View Issue

Cite this: *Soft Matter*, 2024, **20**, 9664

Exploring guest molecule uptake in pH-responsive polyelectrolyte microgels *via* Monte Carlo simulations†

Christian Strauch, Lars Roß and Stefanie Schneider *

Understanding the interactions of guest molecules like proteins and nanoparticles with microgels is fundamental for using microgels as nanocarriers. However, understanding and predicting the system properties becomes increasingly difficult as the systems become more complex. In this study, we systematically investigated the uptake of these guest molecules in a pH-responsive polyelectrolyte microgel modeled as a bead-spring network using Monte Carlo simulations. To narrow down the complexity of the systems, we modeled the guest molecules as simple charged beads. The simulations included the variation of (i) guest molecule charge, (ii) size, and (iii) number, as well as the influence of (iv) the addition of salt. The effect of these parameters on the ionization, swelling, and guest molecule uptake was investigated. The uptake of guest molecules with higher charges enhanced the ionization of the microgel at low pH. The strongest effect was observed for beads with charge z = +15. For higher guest molecule charges, the polymer chains could not fully wrap around the guest molecules, to provide enough microgel charges to fully compensate for the repulsive interactions between the guest beads. In general, the uptake of guest molecules leads to a collapse of the microgel due to attractive electrostatic interactions. With the increasing size of the guest molecules, their excluded volume increases, and the microgel swells with their uptake. Adding monovalent salt slightly decreases the uptake at low ionization of the network due to electrostatic screening. The presence of salt ions with higher valency further decreases the uptake of guest molecules into a fully ionized microgel.

Received 7th August 2024,
Accepted 22nd November 2024

DOI: 10.1039/d4sm00950a

rsc.li/soft-matter-journal

1 Introduction

The targeted delivery of bioactive species to specific locations within biological systems is a major challenge in biomedical applications. Encapsulation of these species in nanocontainers and targeted release has shown promising results.[1–5] Microgels, three-dimensionally crosslinked polymers swollen by a solvent, are suitable candidates for these nanocontainers[6–9] since their swelling behavior and, therefore, their ability to take up guest molecules can be tuned by external stimuli like temperature,[10,11] pH,[12–14] and ionic strength.[15,16] During their encapsulation, the activity of the guest molecule can usually be maintained, which is important in applications like catalysis[17,18] or biosensors.[19–21]

Polyelectrolyte microgels allow the binding with charged guest molecules *via* Coulomb interactions. For weak polyelectrolyte networks, the uptake of guest molecules can be controlled both by pH and ionic strength. For example, an anionic microgel can take up cationic drugs at high pH. In the surroundings of a tumor cell, the pH is decreased, and the drug can then be released since the acidic groups in the microgel will be protonated and uncharged at that pH.[1,3] A further advantage is that the encapsulation of cationic drugs in an anionic microgel lowers their toxicity drastically.[22,23]

Several studies have investigated the uptake and release behavior of proteins in microgels, using cytochrome *c*, a small protein, as a model protein for drug delivery.[24–27] Xu *et al.*[25] investigated the uptake and release of cytochrome *c* in randomly distributed and polyampholyte core–shell microgels. For both systems, uptake took place at a pH of around 8, where cytochrome *c* was positively charged while the polymer networks of the microgels were negatively charged. For the random polyampholytes, repulsive interactions between microgel and cytochrome *c* accelerated the release at lower and higher pH. In contrast, in core–shell microgels, the repulsive interactions between positively charged shell and cytochrome *c* entrapped the cytochrome *c* at low pH.

Wypysek *et al.* investigated the uptake of cytochrome *c* in hollow polyelectrolyte microgels.[26] While the protein molecules were taken up at pH 8, neither the change to pH 4 nor to pH 12

Institute of Physical Chemistry, RWTH Aachen University, Landoltweg 2, 52056 Aachen, Germany. E-mail: schneider@pc.rwth-aachen.de

† Electronic supplementary information (ESI) available. See DOI: https://doi.org/10.1039/d4sm00950a

led to a high amount of released guest molecules. The confinement of the proteins was possibly caused by the high crosslink/monomer ratio of 8%. Additionally, at pH 12 and pH 4, the molecules could be ''released'' into the cavity with the microgel working as a barrier to the surrounding solution, similar to the findings of Xu *et al.* The reduced amount of release at pH 4 could also be explained by higher ionization of the microgel than expected due to the complexation of the proteins.

Cytochrome *c* consists of over 40 acidic and basic units, which can change their charge with pH.[28] Although cytochrome *c* contains hydrophobic residues, the uptake in microgels is mainly driven by electrostatic interactions.[25] Nevertheless, experimentally, it is not easy to systematically investigate the uptake of proteins. In their work, Xu *et al.* supported their experimental findings with Brownian Dynamics simulations. In their model, the charge density of the microgel was fixed. This method can be used if experimental results for the microgel charge are available. However, a prediction of the pH-dependent guest molecule uptake is not possible with this method.

The constant-pH Monte Carlo method is widely used for modeling the pH-dependency in computer simulations.[29] Carnal *et al.*[30–32] and Stornes *et al.*[33] used this method to investigate the complexation of weak polyelectrolyte chains with oppositely charged nanoparticles. Principally, the presence of the nanoparticles was shown to enhance[33] the ionization of the polyelectrolytes, which enabled complexation. However, ionization in microgel systems is more complex since the counterions play an important role. Hofzumahaus *et al.*[34] investigated the influence of microgel concentration, the number of acidic monomers, and the crosslink density on the ionization and swelling behavior of weak polyelectrolyte microgels in salt-free solution showing that the release of counterions strongly impacts ionization and swelling.

The main driving force for the uptake of guest molecules in polyelectrolyte brushes[35,36] and gels[37] is the entropy gain resulting from counterion release. In our recently published work,[38] the counterion release also played an important role in the uptake of titratable oligomers in polyelectrolyte networks. Further, the electrostatic interaction between microgel and oligomers strongly influences the ionization of both microgel and oligomers.

To reduce the complexity of the system, we decided to investigate the uptake of guest molecules with strong charges into a weak anionic polyelectrolyte microgel in this work. We focused on the complex formation caused by Coulomb interactions. To keep the system as simple as possible, we modeled the guest molecules as spherical beads with a fixed positive point charge at their center and a fixed radius. The microgel was modeled as a bead-spring polymer with negatively charged beads, which could change their charge between negatively charged and uncharged during the simulation with the constant-pH method. Based on a reference system (see next section), we systematically varied the number of guest molecules, their charge, and their size. Further, we investigated the influence of ionic strength by adding salt with different concentrations and valencies.

2 Model and simulation parameters

We used the MOLSIM[39] (v.6.4.7) software with extensions by the authors to perform Monte Carlo simulations on a graphics card. Our model is based on previous work,[34,40] in which we modeled microgels using a bead-spring model for the polymer within the primitive model of electrolytes. We extended the model to include positively charged beads for different guest molecules with a radius R_{guest} and negatively charged hard spheres for their counterions. A description of the network generation can be found in ESI,† Section I. Fig. 1 shows a section of a simulation cell. In the following, we will briefly describe the method and potentials used.

In our modeling approach, we utilized the constant-pH method to simulate the pH-dependent behavior of the network. Titratable beads in the simulation could change their charge depending on the pH and their pK value. The pH and the pK value are input parameters, the latter reflecting the acidity of the monomer. According to Reed,[42] the pH was implicitly accounted for by an additional energy term.

$$\Delta U_{ass} = \pm k_B T \cdot \ln(10)(\mathrm{pH} - \mathrm{p}K) \quad (1)$$

in the Metropolis acceptance criterion of the simulation. The plus sign represents the deprotonation of titratable beads, and the minus sign denotes their protonation.

All beads were assigned to a corresponding counterion of opposite charge, changing their charge state together with the network bead to guarantee the electroneutrality of the system. Therefore, a deprotonation step comprised a charge–change from zero to −1 for the acidic beads, while the charge of the counterion changed from zero to +1. In a protonation step, both

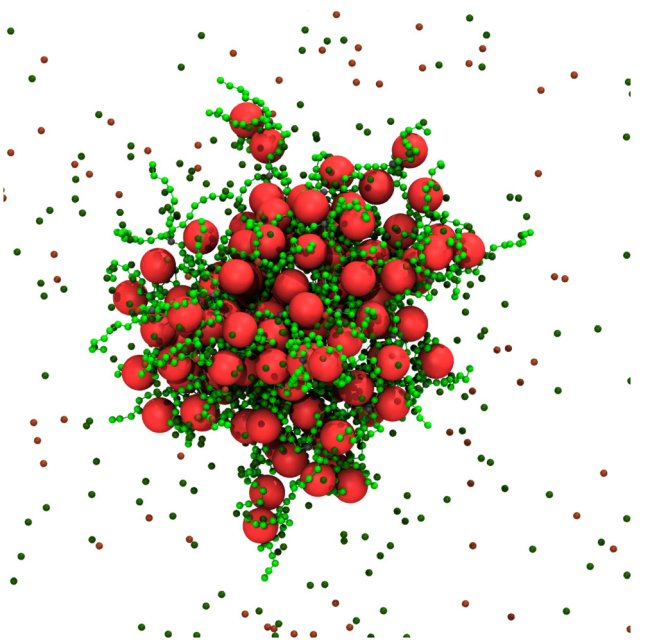

Fig. 1 Snapshot of a simulation cell. The network was modeled as a crosslinked bead-spring polymer. Counterions were considered as explicit beads. Network monomers are light green, their counterions are dark green, the guest molecules are red, and their counterions are brown. The snapshot was generated with VMD.[41]

beads changed their charge to zero. Please note that the implicit treatment of the pH in the constant-pH method misses explicit H^+-ions which can contribute to electrostatic screening. At $3 \leq pH \leq 11$, the missing of explicit ions can be neglected, because both the H_3O^+ as well as the OH^- concentrations are low.

The total potential energy of the system, U_{pot}, was the sum of the pair interactions and the bond energy U_{bond}.

$$U_{pot} = U_{pair} + U_{bond} = \sum_{i<j} u_{ij} + U_{bond} \quad (2)$$

The pairwise additive potential energy is the sum of the potential energy contributions u_{ij} from all pairs of particles. We used a hard-sphere potential for the excluded volume in addition to the Coulomb potential. To account for the long-ranged nature of the electrostatic interactions, we used the Standard Ewald summation technique under periodic boundary conditions (parameters can be found in Table SIV, ESI†).

$$u_{ij}(r_{ij}) = \begin{cases} \infty & r_{ij} \leq R_{i,hs} + R_{j,hs} \\ \dfrac{z_i z_j l_b k_B T}{r_{ij}} & r_{ij} > R_{i,hs} + R_{j,hs} \end{cases} \quad (3)$$

In eqn (3), z_i and z_j are the number of charges of particles i and j, l_b is the Bjerrum length with $l_b = \dfrac{e^2}{4\pi\varepsilon_0\varepsilon_r k_B T}$ and k_B is the Boltzmann constant. The simulations were performed at a temperature of T = 298 K and with a Bjerrum length of $l_b = 3.58\sigma$ (with σ = 2.0 Å) to model an aqueous solution. Accordingly, the dielectric permittivity of ε_r = 78.3 was chosen for these conditions.

The total bond potential energy U_{bond} is the sum of all bond and crosslink energies $u_{ij,bond}$, described with a harmonic spring potential.

$$u_{ij,bond} = \frac{k}{2}(r_{ij} - r_{eq})^2 \quad (4)$$

As force constant, $k = 3.89 k_B T \sigma^{-2}$ was used and the zero-force distance r_{eq} between two bonded beads was given as 2.5σ.

The acceptance probability of a Monte Carlo move was defined by the Metropolis acceptance criterion

$$p_{acc} = \min(1, \exp(-\Delta U_{tot}/(k_B T))). \quad (5)$$

The total energy difference of the system, ΔU_{tot}, was the sum of the potential energy difference, ΔU_{pot}, and the association/dissociation energy difference, ΔU_{ass} given by

$$\Delta U_{tot} = \Delta U_{pot} + \Delta U_{ass}. \quad (6)$$

2.1 Investigated parameters

As a reference system, we chose a system containing 125 guest molecules with a charge of +10 at their centers, resulting in 1250 guest molecule charges. This number corresponds to approximately 75% of the maximum charges of all titratable beads in the microgel which was 1656. The guest molecules had a size of $R_{guest} = 5.0\sigma$. The pK value of the titratable network beads was set to 5.0. The simulations did not contain further added salt, except for the simulations investigated in Section 3.4.

Table 1 Relevant parameters for the discussion of the results

Symbol	Parameter
N_{acid}	Total number of all titratable network beads
N_{guest}	Total number of guest molecules
R_{guest}	Radius of a guest molecule
z_{guest}	Charge of one guest molecule
z_+	Valency of positively charged salt ion
Z_{guest}	Total charge of all guest molecules

Detailed tables with all simulation parameters can be found in Tables SI–SII (ESI†). A brief summary of relevant parameters for discussing the results can be found in Table 1.

In this work, we investigated the following sets of simulations with one parameter (sets 2 and 3) or two parameters (sets 1 and 4) varied compared to the reference system.

1. Numbers and charges of the guest molecules; keeping the total number of guest molecule charges, Z_{guest}, constant.
2. Radius of the guest molecules.
3. Number of the guest molecules, which results in a change in the ratio of Z_{guest} and N_{acid}.
4. Salt concentration and salt cation valence.

2.2 Investigated quantities

The uptake of guest molecules into the polyelectrolyte microgels is mainly determined by the number of charges of the network. The degree of ionization α, which is defined by the number of charged beads of a species divided by the total number of particles of that species, provides quantitative results for the number of charged beads in the networks:

$$\alpha = \frac{\langle N_{acid,ion} \rangle}{N_{acid}} \quad (7)$$

In general, the networks swell more with a higher degree of ionization. On the other hand, the attractive electrostatic interactions between negatively charged polymer beads and positively charged guest molecules lead to a deswelling of the network. As a measure of microgel size, we calculated the radius of gyration R_g of the polymer network.

The number of guest charges taken up by the network $Z_{i,uptake}$ was calculated separately for guest molecules and network counterions by multiplying the number of particles with their respective charge. The number of charged particles taken up was defined by the number of charged particles within a distance to the microgel center of mass equal to the radius of gyration. Additionally, charged beads with a higher distance to the center of mass were counted as taken up if the distance between the charged particle and a network bead was smaller than the Bjerrum length plus their added radii. The effective charge Z_{eff} of the microgel was calculated as the sum of all network charges and all $Z_{i,uptake}$ as

$$Z_{eff} = N_{acid,ion} + \sum_i Z_{i,uptake} \quad (8)$$

Microscopic information was provided by concentration profiles and the degree of ionization as a function of the center of mass of the network. All investigated quantities are summarized in Table 2.

Table 2 Summary of investigated quantities

Symbol	Quantity
α	Degree of ionization in the network
R_g	Radius of gyration of the network
$Z_{i,\mathrm{uptake}}$	Total charge of species i taken up by the network
Z_{eff}	Effective charge of the network-guest-complex including counterions

3 Results and discussion

3.1 Influence of guest molecule charge

In Fig. 2, we show the pH − pK dependence of the degree of ionization α (Fig. 2a), the normalized number of guest molecule charges which are taken up, $Z_{i,\mathrm{uptake}}/N_{\mathrm{acid}}$ (Fig. 2b), the normalized effective microgel charge $Z_{\mathrm{eff}}/N_{\mathrm{acid}}$ (Fig. 2c) on the charge of the guest molecules, as well as the normalized radius of gyration, R_g/σ, (Fig. 2d). The number of charges per guest molecule as well as the number of guest molecules was varied, while the total number of guest charges $Z_{\mathrm{guest}}/N_{\mathrm{acid}} = 0.75$ and the radius of the guest molecules $R_{\mathrm{guest}} = 5\sigma$ was kept constant.

As shown in Fig. 2a, the ionization behavior of the polyelectrolyte network is significantly influenced by the presence of guest molecules with varying charges (z_{guest} = +1 to +20). In the absence of guest molecules (defined as $N_{\mathrm{guest}}/N_{\mathrm{acid}} = 0.000$ in Fig. 2), Hofzumahaus *et al.*[33] showed that the titration curve for the network exhibits a clear shift to higher pH, leading to lower ionization compared to a single monomer at infinite dilution (defined as 'ideal' in Fig. 2). This shift is attributed to unfavorable electrostatic interactions between charged monomers and the titratable unit within the network.

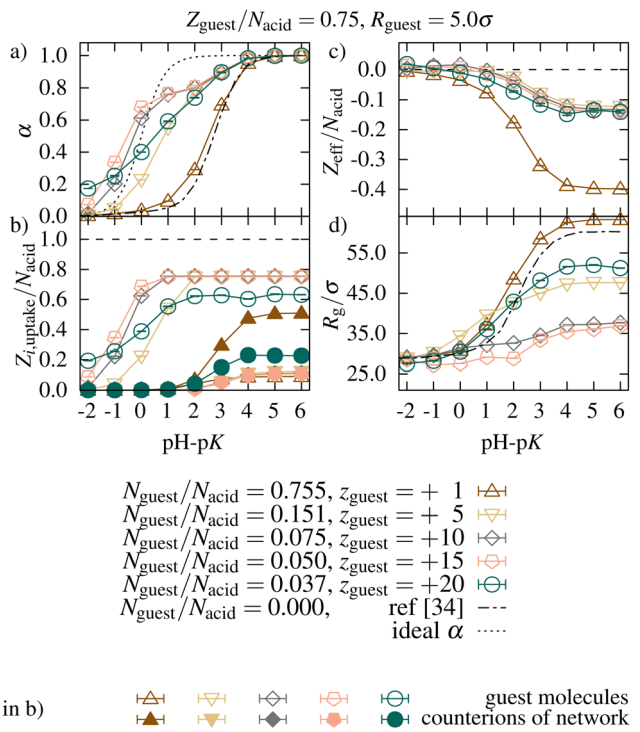

Fig. 2 (a) Degree of ionization of acid within the network for guest molecules with different charges z_{guest}. Lines serve as guidelines. (b) Charges of guest molecules (hollow symbols) and charges of counterions (filled symbols) taken up within the network normalized by the number of bases in the network for guest molecules with different charges z_{guest}.(c) Effective charge as a function of pH − pK. (d) Radius of gyration normalized by bead radius as a function of pH − pK. Data shown as dashed lines were obtained from Hofzumahaus *et al.*[34]

In contrast, the presence of oppositely charged guest molecules leads to an enhanced ionization at intermediate pH− pK. The driving forces for this enhancement are attractive electrostatic interactions between guest molecules and network monomers, as well as the entropic gain from counterion release. For guest molecules with a low charge (z_{guest} = +1), their interaction with the network is weak due to a lower charge density, leading only to a minimal enhancement in ionization attributed to higher ionic strength and higher electrostatic screening. Here, primarily counterions compensate for the network charges (Fig. 2b).

However, guest molecules with a higher charge (z_{guest} = +5 to +15), are taken up by the network more efficiently also leading to an increased network ionization. For z_{guest} = +10 and +15, all guest molecules are taken up at pH − pK ≈ 1 (Fig. 2b), leading to two inflection points in the titration curve. The first steep increase of the ionization can be attributed to the charge compensation by guest molecules, leading to the shift of the ionization curve to lower pH. When all guest molecules are taken up, ionization increases only slowly up to a pH − pK ≈ 2, where a second steep increase is found, which is due to the increased pH and comparable to the increase in α of a network of the same effective charge without guest molecules.

At the highest guest charge (z_{guest} = +20), ionization is enhanced at low pH − pK, but the ionization is lower at intermediate pH − pK compared to z_{guest} = +10 and +15. This can be explained by the smaller uptake of guest molecules caused by the strong repulsive interactions between the guest molecules themselves.

The normalized effective charge of the microgel-guest molecule complex, including counterions, is presented in Fig. 2c. For systems with $z_{\mathrm{guest}} \geq +5$, guest molecule uptake slightly overcompensates the network charge at pH− pK ≈ 0, resulting in a positively charged polymer–guest complex. At pH > pK, the effective charge of the network remains negative due to incomplete compensation by counterions while all guest molecules are taken up.

For z_{guest} = +1, the negative effective charge is higher as fewer guest molecules are taken up. However, for z_{guest} = +20, the effective charge is comparable to the other investigated systems (z_{guest} = +5 to +15) because more counterions within the network compensate for the reduced guest molecule uptake.

The swelling behavior of the polymer network (Fig. 2d) shows that guest molecules with low charge (z_{guest} = +1) lead

to significant swelling at high pH− pK, due to the high effective charge of the network. This swelling exceeds that observed in a salt-free system without guest molecules,[34] which can be attributed to the excluded volume effect of the absorbed guest molecules.

In contrast, for z_{guest} = +5 and z_{guest} = +20, the swelling is more pronounced compared to z_{guest} = +10 and z_{guest} = +15, though the mechanisms differ. In the case of z_{guest} = +5, the swelling is driven by the higher number of guest molecules taken up, which increases the excluded volume within the network. For z_{guest} = +20, the swelling results from strong repulsive interactions between guest molecules, which are localized near the periphery of the network. Additionally, counterions within the microgel create an osmotic pressure that further drives swelling. Moreover, the swelling induced by the increase in osmotic pressure outweighs the deswelling effect caused by electrostatic screening.

3.2 Influence of guest molecule size

A variation of the guest molecule size, while keeping the number of charges per molecule constant, affects the interaction energy of the guest molecule with network monomers in contact. The interaction energy decreases with increasing the guest molecule size. In Fig. 3(a)–(d), the charge per guest molecule, z_{guest} = +10, and their number were kept constant, and only the radius was varied from 2.5σ to 10.0σ. Fig. 3(a) shows that the presence of small guest molecules with R_{guest} = 2.5σ increases the ionization of the network due to stronger electrostatic interactions with the network monomers compared to larger guest molecules. Additionally, more charges are taken up at low pH − pK, which can be seen in Fig. 3(b).

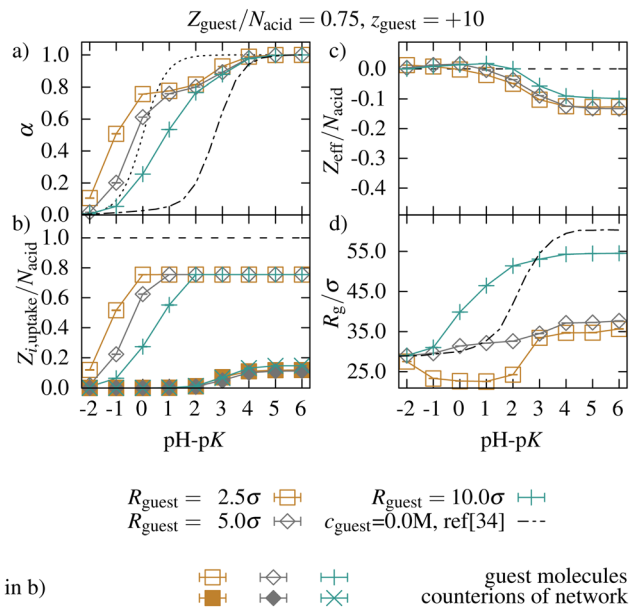

Fig. 3 (a) Degree of ionization of acid within the network for guest molecules with different sizes R_{guest}. Lines serve as guidelines. (b) Charges of guest molecules (hollow symbols) and charges of counterions (filled symbols) taken up within the network normalized by the number of bases in the network for guest molecules with different sizes R_{guest}. (c) Effective charge as a function of pH− pK. (d) Radius of gyration normalized by bead radius as a function of pH − pK. Data shown as dashed lines were obtained from Hofzumahaus *et al.*[34]

The different ionization behavior slightly affects the effective charge shown in Fig. 3(c). At low pH − pK, the effective charge is low, since the network charges are compensated by the guest molecule charges. For guest molecules with R_{guest} = 10.0σ, a positive effective charge can be observed. In the lower pH range, the interactions between the large guest molecules and the network beads are less pronounced. Consequently, the uptake of a guest molecule does not enhance the ionization of the network beads equally much, resulting in an overall excess of guest molecule charges. At high pH − pK, the effective charge is slightly lower for the R_{guest} = 10.0σ compared to the systems with smaller guest molecules, and more counterions are taken up. The higher uptake of counterions can be explained by the larger swelling of the network, which is discussed in the following paragraph.

Besides the electrostatic interactions, the swelling of the network (Fig. 3(d)) is also affected by the excluded volume of the guest molecules. Since the excluded volume of the guest molecules with R_{guest} = 2.5σ is very small compared to that of the larger guest molecules, the attractive interactions between the network and guest molecules lead to a collapse of the network. At high pH − pK, a slight swelling is observed since counterions compensate for the charges in the network at an $\alpha > Z_{guest}/N_{acid} = 0.75$, and the effective charge of the network-guest molecule complex increases. The larger guest molecules cause a large swelling already at low pH − pK. This swelling cannot be explained by the effective charge Z_{eff} but by the high excluded volume (snapshots in ESI,† Fig. S1 illustrate this effect). While this effect is relatively small for R_{guest} = 5.0σ, the excluded volume of guest molecules with R_{guest} = 10.0σ significantly increases the swelling of the network.

3.3 Influence of guest molecule concentration

We varied the total number of guest molecules in a range of 0.30N_{acid} to 1.20N_{acid}. For this variation, Fig. 4 again shows as a function of pH − pK in (a) the degree of ionization, in (b) the number of charges taken up in the network N_{guest}/N_{acid}, in (c) the normalized effective charge of the network-guest complex Z_{eff}/N_{acid}, and in (d) normalized radius of gyration R_g/σ. The uptake of guest molecules caused by Coulomb interactions significantly enhances the ionization compared to a polyelectrolyte network in the absence of guest molecules (dashed lines[34]) as can be seen in Fig. 4(a). At pH− pK = −1, the network takes up the same number of guest molecules independently from the guest molecule concentration (Fig. 4(b)). The uptake enhances the ionization strongly, and it is even increased compared to the ideal ionization at infinite dilution (dotted lines in Fig. 4(a)).

For small guest molecule concentrations, all molecules are already taken up at pH − pK = 0, resulting in a plateau in the ionization curve. Increasing the guest molecule concentration shifts the plateau towards higher pH − pK. The degree of ionization at this plateau approximately equals the total charge of the guest molecules. At pH − pK = 2, the ionization increases,

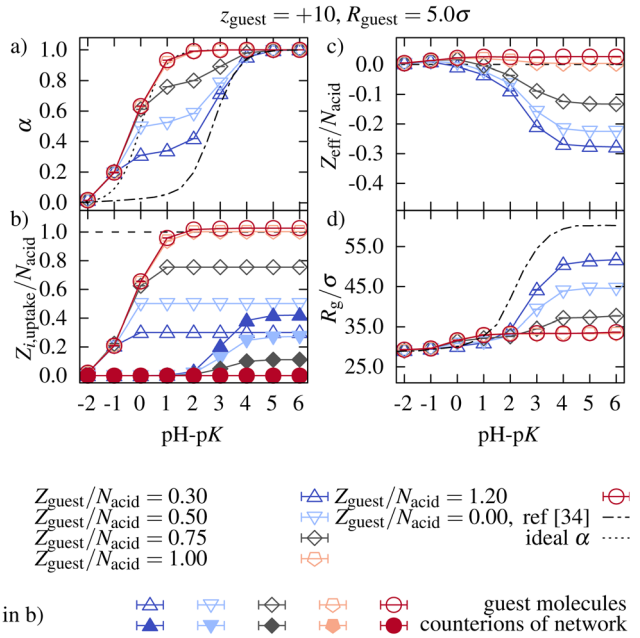

Fig. 4 (a) Degree of ionization of acid within the network for different numbers of guest beads. Lines serve as guidelines. (b) Charges of guest beads (hollow symbols) and charges of counterions (filled symbols) taken up within the network normalized by the number of bases in the network for different numbers of guest beads. (c) Effective charge as a function of pH − pK. (d) Radius of gyration normalized by bead radius as a function of pH − pK. Data shown as dashed lines were obtained from Hofzumahaus *et al.*[34]

and the charges are compensated by counterions. With decreasing the guest molecule concentration, the ionization of the network approaches the curve of the network in the absence of guest molecules. In the case of a total guest molecule charge higher than N_{acid}, no counterions are found within the network.

When the number of ionized network monomers is higher than the total number of guest molecule charges Z_{guest}, network charges must be compensated by counterions. Since the counterion release is entropically favored, a large fraction of the counterions is released, resulting in an effective negative network charge (Fig. 4c). With increasing the guest molecule concentration, the effective charge of the network-guest complex decreases. In the case of Z_{guest}/N_{acid}, the network charge is overcompensated, leading to a positive effective charge of the complex.

As already shown, the swelling of the polymer network relates to the effective charge of the network and the excluded volume of the guest molecules within the network. The larger $|Z_{eff}|$, the larger the radius of gyration, R_g, of the network. Possible explanations for the slight swelling at the highest investigated guest molecule concentration of $Z_{guest}/N_{acid} = 1.2$ in the range of $-1 \leq$ pH − p$K \leq 2$ are (i) the positive effective charge of the complex and (ii) the uptake of more guest molecules, which contribute to the swelling with their excluded volume. A look at the effective charge at pH − pK for the two highest guest molecule concentrations gives additional information that helps to distinguish between the two explanation approaches. For the highest guest molecule concentration, the effective charge is positive while it is almost zero for $Z_{guest}/N_{acid} = 1.0$. However, the radii of gyration are almost the same for both concentrations. This indicates that the excluded volume leads to swelling rather than a positive effective charge.

3.4 Influence of adding salt

Adding salt changes the electrostatic environment and the osmotic pressure of the microgel/guest systems. In general, both electrostatic screening and the Donnan effect can reduce the guest molecule uptake. Fig. 5 shows the influence of salt concentration and the valency of the cationic salt ions on (a) the ionization, (b) the uptake behavior of the network, and (c) the effective charge of the network-guest complex, and (d) the swelling of the network. Besides the salt-free system, we investigated two different salt concentrations of $c_s = 1.0$ mM and $c_s = 5.0$ mM with monovalent salt. Further, we looked at systems containing di- and trivalent cationic salt ions with an ionic strength of $I = 5.0$ mM. The anionic salt ions were kept monovalent for all simulations. At pH − p$K = -1$, both monovalent salt concentrations slightly decrease the ionization of the network in Fig. 5(a). The presence of salt leads to a screening of the electrostatic interactions between guest molecules and the network, which reduces the degree of ionization. However, for pH − p$K \geq 0$, this screening reduces the repulsive interactions between the acidic beads. As a result, the ionization is enhanced compared to the salt-free system.

The electrostatic screening also decreases the uptake of guest molecules at pH − p$K = -1$ shown in Fig. 5(b). The increase of osmotic pressure in the solution by adding salt seems negligible as adding monovalent salt did not reduce the uptake at high pH − pK. The lower charge of the monovalent beads compared to the guest molecules provides an additional explanation for the observation that the presence of monovalent salt does not decrease the uptake of the guest molecules at high pH − pK.

When charge compensation for the network by the guest molecules is reached, the higher osmotic pressure leads to further compensation for network charges by salt ions and, therefore, to additional screening of the network charges. At a fully ionized state, the added salt marginally reduces the effective charge and radius of gyration of the network shown in Fig. 5(c) and (d).

Adding salt with divalent and trivalent cationic ions with an ionic strength of 5.0 mM principally results in an ionization behavior similar to that of the ideal ionization at infinite dilution (dotted lines) due to electrostatic screening. At low pH − pK, the screening decreases the ionization. At pH > pK, monovalent counterions within the microgel are replaced by di- and trivalent salt ions due to the smaller loss in entropy when they are confined to the network, instead of the monovalent ions. This compensation by the salt ions enhances the ionization and decreases the effective charge of the network. Therefore, the radius of gyration is similar to that of the uncharged state.

Adding divalent salt ions does not significantly reduce the uptake of guest molecules. Since one guest molecule can exchange five salt ions to compensate for the network charges, the entropy gain is high enough to ensure complete uptake of

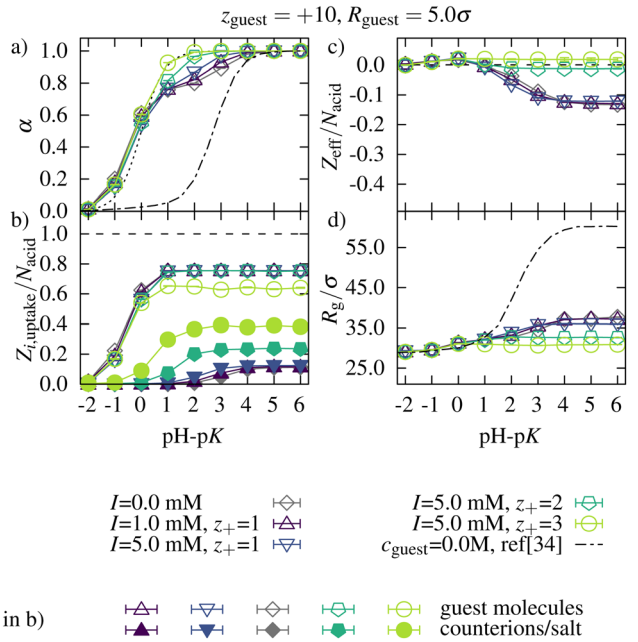

Fig. 5 (a) Degree of ionization of acid within the network in the presence of guest molecules and different salt concentrations and valencies. Lines serve as guidelines. (b) Charges of guest molecules (hollow symbols) and charges of counterions (filled symbols) taken up within the network normalized by the number of bases in the network. (c) Effective charge as a function of pH − pK. (d) Radius of gyration normalized by bead radius as a function of pH − pK. Data shown as dashed lines were obtained from Hofzumahaus *et al.*[34]

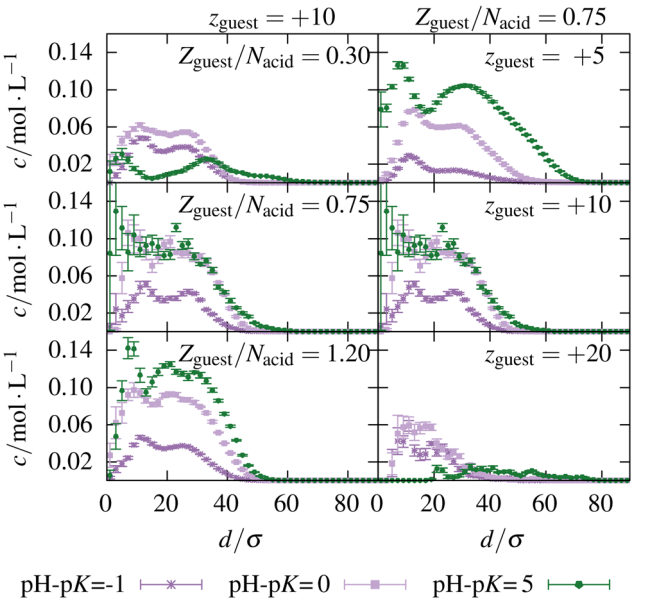

Fig. 6 Concentration profiles of guest molecules for different initial guest molecule concentrations (left) and valencies (right) as a function of distance to the center of mass of the network.

guest molecules. In contrast, the charge of the trivalent salt ions is higher than that for mono- and divalent salt ions. Therefore, fewer salt ions can compensate for the network charges at a high degree of ionization, resulting in a decreased entropic gain by exchanging trivalent salt ions with guest molecules. Furthermore, due to their smaller size, the gain in interaction energy by exchanging trivalent salt ions with guest molecules in the network is strongly decreased. In sum, the reduction of the entropic gain and the reduction in interaction energy gain cause a reduced uptake when adding trivalent salt compared to systems with monovalent salt. The compensation with trivalent ions even overcharges the network for pH > pK. For divalent salt, neither an overcharging for pH > pK nor a decreased uptake was observed.

3.5 Microscopic information

The concentration profiles in Fig. 6 show the concentration of guest molecules as a function of the distance to the network center of mass for different guest molecule concentrations (left) and different guest molecule charges z_{guest} (right). In each panel, three different pH − pK values are considered. The profiles give insight into the number of guest molecules taken up and their distribution within the network. Most of the curves exhibit two maxima and a minimum caused by the regular distribution of crosslinks within the network. Therefore, the maxima and minima are somewhat dependent on how the network is set up initially and should not be paid too much attention to. Nevertheless, they show that the guest particles are preferentially taken up close to the crosslinks inside the network.

At low pH − pK and therefore low degree of network ionization and for the systems with a low guest molecule to monomer ratio, it can be seen, that the guest molecules are first taken up close to the microgel surface and their concentration is much lower in the center of the microgel. This inhomogeneous distribution is caused by an incomplete compensation of guest molecule charges by the network leading to mutual repulsion between the guest molecules. Therefore, the inhomogeneity is most prominent for the guest molecules with the highest charge z_{guest} = +20. Additional swelling of the network further increases the distance of the guest molecules to the center of mass and between themselves.

At higher pH − pK and for larger ratios of Z_{guest}/N_{acid}, the guest molecules are also present closer to the center of the microgel, indicating a more complete charge compensation and complex formation of guest molecule and network. The complexation causes a deformation of multiple chains around a crosslink. These deformations energetically favor the uptake of further guest molecules into these regions. Only for the guest molecules with a charge of z_{guest} = +20, the preferred location of guest molecules in the periphery of the network persists.

The degree of ionization as a function of the distance to the center of mass of the network is shown for three different guest molecule concentrations (left) and three different guest molecule charges (right) at different pH − pK in Fig. 7. For z_{guest} = +10, the ionization within the network is rather homogeneous if the average degree of ionization is smaller than the total charge of the guest molecules (dotted lines) $\alpha \leq Z_{guest}/N_{acid}$. This homogeneous distribution is in contrast to the ionization behavior of a

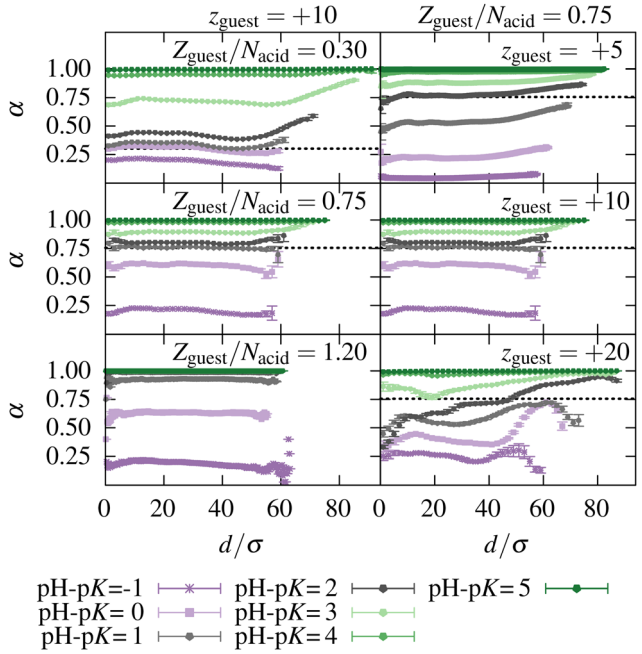

Fig. 7 Degree of ionization of the acids within the network for different pH − pK as function to the distance of the center of mass of the network. Results are shown for different initial guest molecule concentrations (left) and guest molecule charges (right). The dotted lines represent the total charge of the guest molecules.

polyelectrolyte network in the absence of guest molecules, where the ionization is favored in the non-crosslinked dangling chains at the periphery of the network.[33] If the number of ionized monomers exceeds the total guest molecule charges available, also here, the ionization favorably occurs in the dangling chains.

Compared to the ionization at guest molecule charge of z_{guest} = +10, the network shows an overall decreased ionization when decreasing the guest molecule charge to z_{guest} = +5 and the ionization of dangling chains is preferred. While the interaction energy of guest molecules with the charge of z_{guest} = +10 with the network is sufficient to compensate for the repulsive interactions in the core of the network resulting in homogeneous ionization within the network, it seems that the interaction energy of the guest molecules with z_{guest} = +5 with the network is not high enough.

The local ionization shows a more complex behavior in systems with guest molecule charge z_{guest} = +20. At pH − pK = 0, the degree of ionization is approximately constant in the core of the network and increases strongly in the periphery as dangling chains surround the guest molecules. Since the guest molecules bind preferentially close to the crosslinks, the monomers close to the crosslinks are preferred to be ionized (see ESI,† Fig. S3). However, the monomers with the highest distance to the center of mass are not in direct contact with the guest molecules, therefore, less ionized, leading to a decrease in the degree of ionization. At pH − pK = +2, the ionization increases with the distance to the center of mass since the guest molecules, which compensate for the network charges, are located in the periphery.

4. Conclusion

We investigated the uptake of charged guest molecules, modeled as simple charged hard spheres, into pH-responsive microgels using Metropolis Monte Carlo simulations. By varying the number of guest molecules, their charge, and their size, we obtained information about the network ionization and the uptake of the guest molecules into the microgels. We found that the ionization, guest molecule uptake, and microgel volume are determined by a subtle interplay of electrostatic energy, ion entropy, and excluded volume.

Varying the charge of the guest molecules showed three regimes of their uptake. At low charge, the interaction energy of the guest molecule in contact with network monomers is smaller than that of the monovalent counterions. Therefore, uptake is neither energetically nor entropically favored. As a result, only a few of the guest molecules were found inside the microgel.

For guest molecule charges higher than the charge of the counterions, the guest molecules are preferred over counterions to be taken up into the network. The uptake of guest molecules in this regime leads to an increased ionization of the network monomers and, due to complex formation, keeps the network in a collapsed state. The results show that guest molecules in this regime are homogeneously distributed throughout the network. For highly charged guest molecules, the network locally cannot fully compensate for the repulsive electrostatic interactions between the guest molecules, resulting in a decreased uptake and a preferred location of the guest molecules at the microgel periphery.

The size of the guest molecule mainly influences the swelling behavior of the microgel. Due to the larger excluded volume of the bigger guest molecules, the radius of gyration of the network-guest complex, and with this also of the network alone, increases when they are taken up.

Varying the guest molecule concentration (for z_{guest} = +10) showed that with increasing concentration of the guest molecules, the ionization of the network increases significantly at positive pH − pK values.

When monovalent salt is added to the system, the uptake of guest molecules is slightly decreased due to electrostatic screening. For salt ions with higher valency, such as trivalent salt cations, the gain in interaction energy with the network monomers by exchanging trivalent salt ions by guest molecules is strongly decreased, and the gain in entropy by releasing the salt ions is also smaller compared to systems with monovalent salt. Thus, trivalent salt ions compete with the guest molecules and are also present inside the network, leading to a reduction in the guest molecule uptake.

In the future, the model can be extended to more complex structures of guest molecules, including titratable units and short-range attractive interactions.

Author contributions

Christian Strauch: conceptualization, data curation, formal analysis, methodology, software, visualization, writing – original

draft. Lars Roß: data curation, investigation, formal analysis. Stefanie Schneider: conceptualization, supervision, writing – review and editing.

Data availability

Data for this article, including input files, output files, and files with extracted data used for plots, are available at "Dataset belonging to publication 'Exploring guest molecule uptake in pH-responsive polyelectrolyte microgels *via* Monte Carlo simulations'" at **https://doi.org/10.22000/7m1vce62jucq8dvj**.

Conflicts of interest

There are no conflicts of interest to declare.

Acknowledgements

Financial support of the Deutsche Forschungsgemeinschaft within SFB 985 – Functional Microgels and Microgel Systems is gratefully acknowledged. Simulations were performed with computing resources granted by RWTH Aachen University under project rwth0732.

Notes and references

1 S. K. Parks, J. Chiche and J. Pouyssegur, *J. Cell. Physiol.*, 2011, **226**, 299–308.
2 H. Kang, A. C. Trondoli, G. Zhu, Y. Chen, Y. J. Chang, H. Liu, Y. F. Huang, X. Zhang and W. Tan, *ACS Nano*, 2011, **5**, 5094–5099.
3 L. Zha, B. Banik and F. Alexis, *Soft Matter*, 2011, **7**, 5908–5916.
4 Z. Wang, Y. Li, L. Chen, X. Xin and Q. Yuan, *J. Agric. Food Chem.*, 2013, **61**, 5880–5887.
5 Z. Wang, Y. Li, L. Chen, X. Xin and Q. Yuan, *J. Agric. Food Chem.*, 2013, **61**, 5880–5887.
6 A. V. Kabanov and S. V. Vinogradov, *Angew. Chem., Int. Ed.*, 2009, **48**, 5418–5429.
7 F. A. Plamper and W. Richtering, *Acc. Chem. Res.*, 2017, **50**, 131–140.
8 W. Richtering, I. I. Potemkin, A. A. Rudov, G. Sellge and C. Trautwein, *Nanomedicine*, 2016, **11**, 2879–2883.
9 W. Wu, W. Yao, X. Wang, C. Xie, J. Zhang and X. Jiang, *Biomaterials*, 2015, **39**, 260–268.
10 M. Zeiser, I. Freudensprung and T. Hellweg, *Polymer*, 2012, **53**, 6096–6101.
11 M. Quesada-Pérez, J. Ramos, J. Forcada and A. Martín-Molina, *J. Chem. Phys.*, 2012, **136**, 244903.
12 C. D. Jones and L. A. Lyon, *Macromolecules*, 2000, **33**, 8301–8306.
13 C. D. Jones and L. A. Lyon, *Macromolecules*, 2003, **36**, 1988–1993.
14 S. Schachschal, A. Balaceanu, C. Melian, D. E. Demco, T. Eckert, W. Richtering and A. Pich, *Macromolecules*, 2010, **43**, 4331–4339.
15 D. Capriles-González, B. Sierra-Martín, A. Fernández-Nieves and A. Fernández-Barbero, *J. Phys. Chem. B*, 2008, **112**, 12195–12200.
16 A. Moncho-Jordá, J. A. Anta and J. Callejas-Fernández, *J. Chem. Phys.*, 2013, **138**, 134902.
17 M. Nöth, L. Hussmann, T. Belthle, I. El-Awaad, M. D. Davari, F. Jakob, A. Pich and U. Schwaneberg, *Biomacromolecules*, 2020, **21**, 5128–5138.
18 R. Borrmann, V. Palchyk, A. Pich and M. Rueping, *ACS Catal.*, 2018, **8**, 7991–7996.
19 L. V. Sigolaeva, S. Y. Gladyr, A. P. H. Gelissen, O. Mergel, D. V. Pergushov, I. N. Kurochkin, F. A. Plamper and W. Richtering, *Biomacromolecules*, 2014, **15**, 3735–3745.
20 S. Su, M. M. Ali, C. D. M. Filipe, Y. Li and R. Pelton, *Biomacromolecules*, 2008, **9**, 935–941.
21 M. R. Islam, A. Ahiabu, X. Li and M. J. Serpe, *Sensors*, 2014, **14**, 8984–8995.
22 L. Chen, J. D. Simpson, A. V. Fuchs, B. E. Rolfe and K. J. Thurecht, *Mol. Pharmaceutics*, 2017, **14**, 4485–4497.
23 G. Agrawal, R. Agrawal and A. Pich, *Part. Part. Syst. Charact.*, 2017, **34**, 1700132.
24 M. H. Smith and L. A. Lyon, *Macromolecules*, 2011, **44**, 8154–8160.
25 W. Xu, A. A. Rudov, R. Schroeder, I. V. Portnov, W. Richtering, I. I. Potemkin and A. Pich, *Biomacromolecules*, 2019, **20**, 1578–1591.
26 S. K. Wypysek, S. P. Centeno, T. Gronemann, D. Wöll and W. Richtering, *Macromol. Biosci.*, 2023, **23**, 2200456.
27 I. K. Sommerfeld, H. Malyaran, S. Neuss, D. E. Demco and A. Pich, *Biomacromolecules*, 2024, **25**, 903–923.
28 Y. Mao, M. A. Ratner and M. F. Jarrold, *J. Phys. Chem. B*, 1999, **103**, 10017–10021.
29 J. Landsgesell, L. Nová, O. Rud, F. Uhlík, D. Sean, P. Hebbeker, C. Holm and P. Košovan, *Soft Matter*, 2019, **15**, 1155–1185.
30 F. Carnal and S. Stoll, *J. Phys. Chem. B*, 2011, **115**, 12007–12018.
31 F. Carnal, A. Clavier and S. Stoll, *Environ. Sci.: Nano*, 2015, **2**, 327–339.
32 F. Carnal, A. Clavier and S. Stoll, *Polymers*, 2016, **8**, 203.
33 M. Stornes, P. Linse and R. S. Dias, *Macromolecules*, 2017, **50**, 5978–5988.
34 C. Hofzumahaus, P. Hebbeker and S. Schneider, *Soft Matter*, 2018, **14**, 4087–4100.
35 A. L. Becker, K. Henzler, N. Welsch, M. Ballauff and O. Borisov, *Curr. Opin. Colloid Interface Sci.*, 2012, **17**, 90–96.
36 X. Xu, S. Angioletti-Uberti, Y. Lu, J. Dzubiella and M. Ballauff, *Langmuir*, 2018, **35**, 5373–5391.
37 A. M. Rumyantsev, S. Santer and E. Y. Kramarenko, *Macromolecules*, 2014, **47**, 5388–5399.
38 C. Strauch and S. Schneider, *Soft Matter*, 2024, **20**, 1263–1274.
39 J. Reščič and P. Linse, *J. Comput. Chem.*, 2015, **36**, 1259–1274.
40 C. Strauch and S. Schneider, *Soft Matter*, 2023, **19**, 938–950.
41 W. Humphrey, A. Dalke and K. Schulten, *J. Mol. Graphics*, 1996, **14**, 33–38.
42 C. E. Reed and W. F. Reed, *J. Chem. Phys.*, 1992, **96**, 1609–1620.

